AD-A188 308 FURTHER REFINEMENT AND APPLICATIONS OF THE MIXED COMPUTATIONAL ALGORITHM F (U) VIRGINIA POLYTECHNIC INST AND STATE UNIV BLACKSBURG DEPT OF E 1/1

UNCLASSIFIED E YOGESWAREN ET AL OCT 87 VPI-E-87-25 F/G 13/5 NL

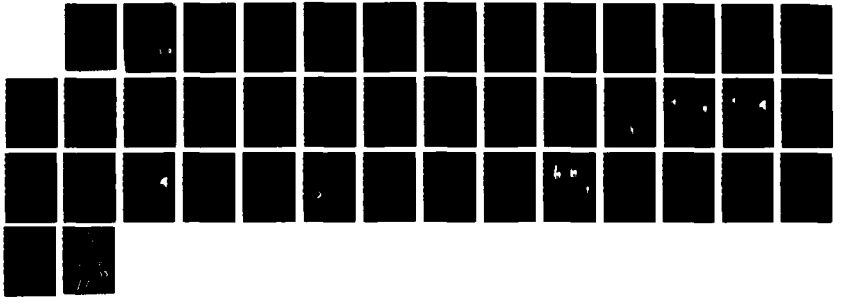

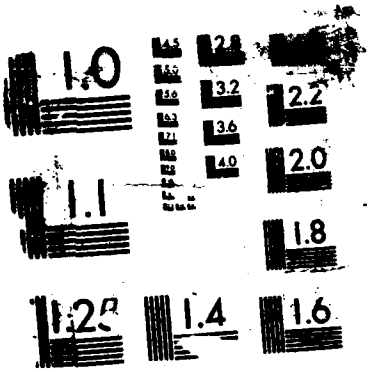

MICROCOPY RESOLUTION TEST CHART

Department of the Navy
OFFICE OF NAVAL RESEARCH
Mechanics Division
Arlington, Virginia 22217

Contract N00014-84-K-0552
Project NR 064-727/5-4-84 (430)

Research Report No. VPI-E-87.25

FURTHER REFINEMENT AND APPLICATIONS OF THE MIXED COMPUTATIONAL ALGORITHM FOR PLANE ELASTIC CONTACT PROBLEMS

by

E. Yogeswaren and J. N. Reddy
Department of Engineering Science and Mechanics
Virginia Polytechnic Institute and State University
Blacksburg, VA 24061

October 1987

TABLE OF CONTENTS

ABSTRACT

TABLE OF CONTENTS

1. INTRODUCTION..... 1

2. PRESENT STUDY 3
   2.1 Contact Stress Evaluation..... 3
   2.2 Modified Solution Technique..... 6

3. LITERATURE REVIEW..... 7
   3.1 Overview..... 7
   3.2 Eulerian-Lagrangian Description for Severe Deformation and Fracture..... 9
   3.3 Failure Analysis of Mechanical Joints 11

4. APPLICATIONS..... 12
   4.1 A Pin-Loaded Aluminum Plate..... 12
   4.2 A Pin-Loaded Orthotropic Plate..... 14
   4.3 Application of the Hybrid Technique to Estimate Static and Dynamic Coefficients of Friction..... 15
   4.4 Analysis of Failure in Mechanical Joints..... 15

5. SUMMARY AND CONCLUSIONS..... 16

REFERENCES..... 18

FIGURES..... 20

FURTHER REFINEMENT AND APPLICATIONS OF THE MIXED COMPUTATIONAL ALGORITHM FOR PLANE ELASTIC CONTACT PROBLEMS

E. Yogeswaren* and J. N. Reddy‡
Department of Engineering Science and Mechanics
Virginia Polytechnic Institute and State University
Blacksburg, VA 24061

ABSTRACT

The mixed finite element scheme developed earlier has been further studied in order to improve the model characteristics and operation as well as to explore further applications with regards to mechanical joints. One of the important modifications that has been implemented in the present study is the utilization of a dynamic as well as a static coefficient of friction for the evaluation of contacting surface behavior instead of a single friction coefficient as used in the previous study. This has improved the model behavior and involved a substantial reorganization of program methodology. Other refinements include the incorporation of a modified solution technique that allows the solution of the indefinite stiffness equation system which is formed in the first iteration of the first load step, and the usage of a finer mesh. The new solution technique also avoids the halt of execution of the program whenever small elements are introduced in the leading diagonal due to contact loss.

The case of the pin-loaded aluminum plate has been studied again to obtain better correlation with experimental results; and a pin-loaded orthotropic plate behavior as predicted by an analytical solution is compared with the present model predictions. The hybrid technique has been used to estimate the static and dynamic coefficients of friction of the aluminum pin/plate system.

An elastic-plastic analysis based failure model of pin-loaded laminates is illustrated by examples which indicate when bearing, shearout and tensile failure occur in the laminate mechanical joints. Finally, some improvements that could be carried out on the present model to predict severe deformation and fracture behavior are discussed.

---

*Graduate Research Assistant

‡Clifton C. Garvin Professor of Engineering Science and Mechanics

1. INTRODUCTION

The updated Lagrangian formulation based on a mixed variatonal statement and the associated finite element model developed earlier [1] gave results in good agreement with the analytical solutions for most contact problems studied there. However, the numerical results obtained for the pin-loaded aluminum plate showed poor correlation with the experimental results of Joh [2]. The poor correlation can be attributed to both theoretical and experimental models used. It was also discovered that the need for a better solution technique existed since the program operation was disrupted whenever certain contact node pairs were about to lose contact thus creating very small terms in the leading diagonal. The work reported here is largely based on the subsequent research carried out to improve the accuracy of the results by modifying and refining the computational procedure developed earlier. Applications of the refined model to the pin-loaded plate problem and other contact problems such as a mechanical joint in filamentary composite laminates are presented.

Factors responsible for the discrepancy between the theoretical and experimental results can be many and may include the non-ideal conditions under which the experiment was conducted. An attempt is made in the present study to see if closer agreement between the theoretical and experimental results can be achieved by refining the computational model. Indeed, the study showed that it is possible if a dynamic coefficient of friction (μ_d) and a static coefficient of friction (μ_s) are used in the analysis instead of a single coefficient of friction, as was done in the earlier work. This approach is more realistic since this comes closer to the continuously varying friction coefficient

observed in practice. The basis for the values of μ_d and μ_s is provided by the hybrid technique study conducted with the experimental values of displacements along the hole boundary.

It was reported in [1] that the first node of the finite element mesh was selected as to be constrained in both directions which enables the use of a conventional banded solver. This is due to the fact that the leading diagonal terms in $[K^{11}]$ (see [1]) will be zero in the first iteration of the first load increment, thus giving an indefinite system of equations. Although this simple solution worked for problems with carefully chosen mesh numbering, it breaks down when leading diagonal terms become small due to loss of contact between pairs of nodes. Hence, the earlier solution scheme was discarded in favor of the technique suggested by Mirza [3].

In addition to the above modifications, which are mainly remedial in nature, some applications of the refined model were also conducted particularly with respect to failure in mechanical joints of composites. The advantages and pitfalls of the technique are also outlined in the section on applications.

Finally, an alternative kinematic description is suggested for severe deformations and cracks encountered in contact systems. This model when incorporated in the present scheme can lead to economical analyses of large deformation problems with fracture by avoiding the remeshing techniques normally used in these cases. No attempt is made to implement the computational procedure in the present study.

2. PRESENT STUDY

2.1 Contact Stress Evaluation

Evaluation of the kinematical relations and tractions at the contacting surface is a significant factor in the analysis of contact problems. One of the main advantages accrued from mixed formulation is that the normal and tangential surface tractions can be calculated directly from the nodal stress values obtained in the mixed model. A practical way of treating contact surfaces is to assume that the forces are transferred only at the nodal points as concentrated forces resulting from the integrated effect of contact stresses up to and including the contactor node. In the earlier work [1] a segment of triplet nodes were considered on the contactor body, with the node in consideration as the middle node, and by integrating the tractions on the contactor surface the nodal forces were obtained. In the present study a more direct and simple algorithm is adopted to reduce calculations involved and by using a finer mesh it is made certain that the accuracy of the model is not compromised.

In the present analysis the contact status of any contact segment of the target body containing a node of the contactor is decided by the normal and tangential nodal forces at the given node. If the tangential force at a node is more than the frictional capacity then the node is under sliding contact. The limiting frictional resistance that can be sustained by a stationary node K is given by,

$$\begin{pmatrix}\text{Static}\\ \text{Frictional}\\ \text{Capacity}\end{pmatrix}_K = \begin{pmatrix}\text{Static Coefficient}\\ \text{of friction } \mu_s\end{pmatrix} \times \begin{pmatrix}\text{Normal Force}\\ \text{Component}\\ \text{at node K}\end{pmatrix}. \quad (2.1)$$

However, if there is already slip occurring in the last load increment, the frictional capacity is given by

$$\left(\begin{array}{c}\text{Dynamic}\\ \text{Frictional}\\ \text{Capacity}\end{array}\right)_K = \left(\begin{array}{c}\text{Dynamic Coefficient}\\ \text{of Friction } \mu_d\end{array}\right) \times \left(\begin{array}{c}\text{Normal Force}\\ \text{Component}\\ \text{at Node K}\end{array}\right). \quad (2.2)$$

Although the above concept was discussed in [1], it was left to the current study to implement this into the program. Thus as a first step, the direct path discussed in this section was chosen to check the usefulness of this notion. It should be noted here that Sections 3.3.4 and 3.3.5 of [1] are made obsolete by the present approach. But, implementation of μ_s and μ_d in the integration process outlined in these sections will be carried out if the present method is found to be unsatisfactory in later applications.

Sticking contact occurs if the frictional capacity as determined by Eq. (2.1) or Eq. (2.2) exceeds the tangential force at node K. The conditions of contact from the last load increment determines whether Eq. (2.1) or Eq. (2.2) is used. Any free target segment that comes in contact will have a sticking contact since the tangential force is zero along the free surface. This is also true when a segment re-establishes contact after a separation. However, when the friction coefficient is very low the frictional capacity may be so low that sliding may occur at initial contact itself.

Sliding condition is brought about when the nodal tangential force exceeds the frictional capacity of the segment given by the appropriate equation (2.1) or (2.2). The node is constrained to move only in the tangential direction and the frictional resistance opposes the relative motion of the bodies. The dynamic frictional resistance opposing the motion changes continuously as a function of the relative magnitude of the tangential and normal forces acting at a given node. As a first-order approximation, the value of the resistance at the beginning of the

load increment is assumed to be opposite to the direction of motion. It is to be noted that the global nodal forces are the external forces acting on every element to balance the forces due to the stresses. Frictional forces are externally applied at the contactor nodes in the direction of tangential force and are given by,

$$(\text{External Frictional Forces})_K = \text{sign}\left(\begin{matrix}\text{tangential}\\ \text{nodal force}\end{matrix}\right)_K \times \mu_d \times \left(\begin{matrix}\text{normal}\\ \text{nodal}\\ \text{force}\end{matrix}\right) \tag{2.3}$$

if and only if

$$\left|\begin{matrix}\text{Normal}\\ \text{Nodal Force}\end{matrix}\right| \leq \left|\begin{matrix}\text{Tangential}\\ \text{Nodal Force}\end{matrix}\right| . \tag{2.4}$$

The frictional force is determined at all equilibrium configurations and applied along the target surface.

When the coefficient of friction is very small the frictional capacity of all the segments under contact is identically zero at all times. The contactor nodes follow the fixed target surface and since the target surface need not be parallel to the global axes, a local coordinate system is defined with constraint of movement along one axis.

Separation occurs when the reactive contact forces act in the negative direction of the unit outward normal to the contact surface. However, if the forces as evaluated at the end of an equilibrium configuration become positive, then there is no contact force betwen the contacting bodies, and the segment containing the node has separated. This node is considered to be free and once again is a potential contactor node and checked for contact overlap in subsequent load increments.

2.2 Modified Solution Technique

The finite element equations resulting from the mixed formulation can be written as,

$$\begin{bmatrix} [K^{11}] & [K^{12}] \\ [K^{12}]^T & [K^{22}] \end{bmatrix} \begin{Bmatrix} \{u\} \\ \{S\} \end{Bmatrix} = \begin{Bmatrix} \{F\} \\ \{0\} \end{Bmatrix} \tag{2.5}$$

where

$$K_{ij}^{11} = \int_{\Omega} \left[\tau_{xx} \frac{\partial \psi_i}{\partial x} \frac{\partial \psi_j}{\partial x} + \tau_{xy} \left(\frac{\partial \psi_i}{\partial x} \frac{\partial x_j}{\partial y} + \frac{\partial \psi_i}{\partial y} \frac{\partial \psi_j}{\partial x} \right) + \tau_{yy} \frac{\partial \psi_i}{\partial y} \frac{\partial \psi_j}{\partial y} \right] dxdy \tag{2.6}$$

Thus it can be seen from Eq. (2.6), for the first iteration of the first load increment, that $[K^{11}] = 0$ because $\tau_{xx} = \tau_{xy} = \tau_{yy} = 0$, thus resulting in an indefinite system of equations. Although Eq. (2.5) can be solved for this condition, by first solving for stress and then for displacements, a more direct way has been given by Mirza [3]. He suggested that premultiplying both sides of the equation by the transpose of the global stiffness matrix, one can obtain a positive-definite system of equations. For example, if Eq. (2.5) can be written as

$$[K][\delta] = [P] \tag{2.6}$$

where

$$[K] = \begin{bmatrix} [0] & [K^{12}] \\ [K^{12}]^T & [K^{22}] \end{bmatrix}, \quad \{\delta\} = \begin{Bmatrix} \{u\} \\ \{S\} \end{Bmatrix} \times \{P\} = \begin{Bmatrix} \{F\} \\ \{0\} \end{Bmatrix},$$

then a positive definite system is given by

$$[K]^T[K]\{\delta\} = [K]\{P\}, \tag{2.7}$$

and the solution of Eq. (2.7) gives the results of Eq. (2.6).

This technique has been extended in the present study by reforming Eqs. (2.5) into the type given by Eq. (2.6) whenever leading diagonal terms are small and then carrying out the operations described above.

3. LITERATURE REVIEW

3.1 Overview

The earlier work [1] contains and discusses a number of references on the finite element analyses of contact problems and the present review is intended to be within the scope of the present study. The major aspects of contact problems have been discussed in detail in [1] and it would be appropriate here to concentrate on how the model can be improved by modifications based on an Eulerian-Lagrangian formulation as discussed in [4-6], and to examine some of the work that has been carried out on the failure of mechanical joints in composites.

Mixed formulations of contact problems can be further enhanced by incorporating a form of kinematic description, addressed in [4] as an Eulerian-Lagrangian displacement model. The conventional Lagrangian description uses a fixed reference material configuration to formulate equilibrium equations where a certain reference quantity of material is "followed" throughout its physical behavior. Conversely, the material can be allowed to "flow" across a fixed spatial reference and physical measurements can be referred to the fixed frame. The total Lagrangian description uses initial configuration as the reference whereas the updated Lagrangian description refers to the current deformed state. But the General Lagrangian description and Eulerian-Lagrangian description are more flexible in that the configurations used to measure spatial variables and to define the strain measure need not be the same. Thus, this allows material flow across the meshes thus enabling

large deformations in contact and fracture to be captured within an initial mesh rather than employing mesh redefining techniques. The application of this technique is illustrated in [5] for contact problems and in [6] for dynamic fracture problems.

Calculation of the strength and failure mode of a composite laminate containing a pin-loaded hole requires the knowledge of the load distribution inside the surface of the hole. Frequently, a cosine load distribution is assumed sirce such a load distribution greatly simplifies the calculations. The stresses inside the laminate calculated by a cosine load distribution may differ significantly from those which actually arise in the structure. As a result, those failure criteria which require an accurate knowledge of the stress distributions near the surface of the hole, will predict failure inaccurately when used in conjunction with cosine load distribution. Work on composite bolted joints has been extensive with early studies concentrating on empirical design and gradually progressing to analytical methods for stress analysis (see [7-14]) and the search for appropriate failure criteria (see [15-20]). Empirical design methods proved too costly and time consuming since the large number of variables in joint design require huge data bases for each material and class of laminates. Thus analytical techniques have been attractive, although this requires vigilance on the part of the designer towards the pitfalls normally encountered.

3.2 Eulerian-Lagrangian Description for Severe Deformation and Fracture

This section reviews the updated Lagrangian scheme used in the present study, and outlines the Eulerian-Lagrangian formulation for an easier and accurate modelling of contact and fracture. However, the latter scheme is not implemented on the computer during the present research.

The modified functional with the Lagrange multiplier for the updated Lagrangian formulation is given by (see [1]),

$$\pi_L = \int_{v_1} \frac{1}{2}\, {}^1C_{ijrs}\, {}^1e_{rs}\, {}^1e_{ij}\, dv + \int_{v_1} {}^1\tau_{ij}({}^1e_{ij} + {}^1\eta_{ij})dv - {}^1F$$

$$- \int_{v_1} {}^1S_{ij}[{}^1e_{ij} - \frac{1}{2}\,(\frac{\partial u_i}{\partial x_j} + \frac{\partial u_j}{\partial x_i})]dv \qquad (3.1)$$

$$\text{Since } {}^1S_{ij}\, {}^1e_{ij} = U_o^* + \frac{1}{2}\, C_{ijk\ell}\, {}^1e_{ij}\, {}^1e_{k\ell} \qquad (3.2)$$

Eq. (3.1) can be expressed as

$$\pi_L = \int_{v_1} [\tau_{ij}(e_{ij} + {}^1\eta_{ij}) + \frac{1}{2}\, {}^1S_{ij}(\frac{\partial u_i}{\partial x_j} + \frac{\partial u_j}{\partial x_i}) - U_o^*]dv - {}^1F \qquad (3.3)$$

where U_o^* the complementary strain energy density,

$$U_o^* = \frac{1}{2}\, D_{ijk\ell}\, {}^1S_{ij}\, {}^1S_{k\ell} \qquad (3.4)$$

By imposing stationarity on π_L in Eq. (3.3), we obtain the following two apprximate equilibrium equations which form the basis of the mixed finite-element model:

$$\int_{v_1} {}^1\tau_{ij}\delta({}^1\eta_{ij})dv + \int_{v_1} {}^1S_{ij}\delta u_{i,j}\, dv = \delta({}^1F) = \int_{v_1} {}^1\tau_{ij}\delta({}^1e_{ij})dv \qquad (3.5)$$

$$\int_{v_1} u_{i,j}\delta({}^1S_{ij})dv = \int_{v_1} D_{ijk\ell}\, {}^1S_{k\ell}\delta({}^1S_{ij})dv = 0\ . \qquad (3.6)$$

Approximating the displacements and stresses by

$$u_i(x_1,x_2) = \sum_{j=1}^{n} u_i^j \psi_j(x_1,x_2) \tag{3.7}$$

$$ {}^1S_{ij}(x_1,x_2) = \sum_{k=1}^{n} {}^1S_{ij}^k \psi_k(x_1,x_2) \tag{3.8}$$

and substituting Eqs. (3.7) and (3.8) into Eqs. (3.5) and (3.6), we obtain the mixed finite element model,

$$\begin{bmatrix} [K^{11}] & [K^{12}] \\ [K^{12}]^T & [K^{22}] \end{bmatrix} \begin{Bmatrix} \{u\} \\ \{S\} \end{Bmatrix} = \begin{Bmatrix} \{F\}^L \\ 0 \end{Bmatrix} - \begin{Bmatrix} \{F\}^{NL} \\ 0 \end{Bmatrix}, \tag{3.9}$$

where the details of the element matrices are given in [1].

A similar approach with the Eulerian-Lagrangian model would give,

$$\Pi_L = \frac{1}{2} \int_{V^R} ({}^1\tau_{ij} + {}^1S_{ij})({}^1e_{ij} + {}^1\eta_{ij})\tilde{J}dV_R$$

$$- \int_{V^R} {}^1S_{ij}[{}^1e_{ij} - \frac{1}{2}(\frac{\partial u_i}{\partial x_k^R}\tilde{J}_{kj} + \frac{\partial u_j}{\partial x_k^R}\tilde{J}_{ki})]\tilde{J}dV_R \tag{3.10}$$

where

$$\tilde{J}_{kj} = \frac{\partial x_k^R}{\partial X_j} \quad \text{and} \quad \tilde{J} = \left|\tilde{J}_{ij}\right| .$$

Similar manipulations as for the updated Lagrangian formulation lead to,

$$\begin{bmatrix} [K'_{11}] & [K'_{12}] & [K'_{13}] \\ [K'_{21}] & [K'_{22}] & [K'_{23}] \\ [K'_{31}] & [K'_{32}] & [K'_{33}] \end{bmatrix} \begin{Bmatrix} \{u\} \\ \{U\} \\ \{S\} \end{Bmatrix} = \begin{Bmatrix} \Delta R'_1 \\ \Delta R'_2 \\ \Delta R'_3 \end{Bmatrix} \tag{3.11}$$

where $\{u\}$ is the Lagrangian incremental displacement, $\{U\}$ is the Eulerian incremental displacement, and $\{S\}$ is the incremental stress vector. The total incremental displacement is given by

$$\{U_T\} = \{u\} - \{U\} \tag{3.12}$$

The details of the Eulerian-Lagrangian method and its application in the present context can be found in [4] for the contact model and in [6] for the fracture model, although References 4 and 6 consider only the displacement formulations.

3.3 Failure analysis of Mechanical Joints in Composites

Stress analysis, a failure criterion and a strength model are the basic components of a joint failure analysis (or a strength analysis). The three basic failure modes associated with bolted joints in composites are the bearing failure, the shearout failure and the net tensile failure (see [15-37] and [18-23]). It has been found that the shearout and the net tensile failure can be adequately modelled by a plane elastic stress analysis, with a point stress failure hypothesis and a macroscopic failure model such as the maximum stress or the maximum strain criterion.

Recently, there is a trend towards studies incorporating ply-by-ply failure analysis of bolted joints, in order to assess the damage to individual plies (see Reddy and Pandey [24]). This requires some form of macroscopic criterion such as the Tsai-Hill or Hoffman's criterion to predict failure.

An altogether different approach has been adopted towards failure by Hyer et al. ([7],[8]), who have used the maximum radial and circumferential stresses as indicators of the capacity of a bolted joint in order to study the effects of pin elasticity, pin fit-interference and friction on the capacity of a joint. They concluded that all three factors are detrimental to the capacity of the bolted joint.

4. APPLICATIONS

4.1 A Pin-Loaded Aluminum Plate

Three different meshes were used to model the aluminum plate. All meshes took advantage of the symmetry of the problem and modelled only half the plate. Further simplification was carried out on Mesh A (Fig. 1), where only a quarter of the pin was modelled as was discussed in the earlier study [1]. However, both Mesh B and Mesh C did not adopt this simplification and they modelled half the pin as shown. The contact nodal locations of Mesh A are reiterated here for completeness. These locations are the following (degrees): 0.0, 1.0, 2.0, 4.0, 6.0, 8.0, 10.0, 12.5, 15.0, 20.0, 25.0, 30.0, 35.0, 40.0, 45.0, 54.0, 63.0, 72.0, 90.0, 99.0, 108.0, 117.0, 126.0, 135.0, 144.0, 153.0, 162.0, 171.0 and 180.0. In Mesh B these locations were spaced at 9° intervals and in Mesh C these were at 2.5° intervals for the first 90° and at 9° intervals for the second 90° as shown in Fig. 2 and 3 respectively. The number of elements and the nodes in the meshes are given as follows:

Mesh A: 236 elements, 286 nodes,

Mesh B: 332 elements, 391 nodes,

Mesh C: 452 elements, 540 nodes.

All nodes along the line of symmetry were constrained to move only in the lengthwise direction and the center of the pin (numbered 1) in all three meshes was constrained in both directions. The load applied was distributed along the shorter edge away from the pin, in the lengthwise direction. A dynamic coefficient of friction $\mu_d = 0.25$ and a static coefficient of friction $\mu_s = 0.35$ were used in the analysis with these numerical values having been estimated from the hybrid technique.

The load was applied in 14 steps following closely the experimental loading values. In the load increasing phase the values of load were 20, 23, 520, 1240, 1460, 1670 and 1980 lbs. respectively with the decreasing phase values being 1800, 1600, 1210, 1070, 535, 210 and 40 respectively giving 14 load steps. The number of iterations required for each load increment were 8, 8, 3, 3, 3, 1, 2, 2, 2, 3, 2, 3, 3, and 3 for the case illustrated in Fig. 6, where Mesh A was used and results are plotted for load step 4, where the total load is at a value of 1240 lbs.

The case shown in Fig. 5 was analyzed with the modified computational procedure discussed in Section 2. The results show a closer agreement with the experimental results of Joh [2], than the results shown in Fig. 4, which were obtained using the original procedure of [1]. It is interesting to note that a constant value of friction coefficient of 0.15 gives a closer agreement in Fig. 4 than the constant friction coefficient of 0.30, these values being chosen arbitrarily. It is possible here to be misled easily to conclude that a better choice of value of friction coefficient might be 0.15 than 0.30 unless the full picture is revealed by Fig. 5, which indicates that better results are given by a dynamic/static friction model. Indeed it is possible to conclude here that yet better modelling can be achieved by a continuous friction coefficient variation such as that given by a power law although the implementation of this may be more cumbersome. It can also be seen that the angle of separation is more realistic in Fig. 5 (after the modification) than in Fig. 4 (before the modification).

The load decreasing phase results shown in Fig. 6 compare favorably with the experimental results, despite some 66% difference in the values of $\tau_{r\theta}$ from 40° to 75°. This can be considered fair compared to the results given by the method before modification, which gave identical results to the load increasing phase without any negative values for $\tau_{r\theta}$.

4.2 A Pin-Loaded Orthotropic Plate

An analytical solution to the problem of pin-loaded composite laminate has been obtained by Hyer et al. ([7],[8]) based on a complex Fourier series method and a collocation technique which enforced boundary conditions at discrete locations around the hole boundary. Results were obtained by this analytical method for infinite orthotropic plates loaded by pins. These results were chosen to be compared with the finite element results since both methods capture the idealized conditions of the model to the same degree.

The mesh shown in Fig. 7 was selected to idealize the infinite plate and the pin, with 426 elements and 509 nodes. The nodes along the line of symmetry were constrained to move only in the lengthwise direction in the same way as the nodes along the longer boundary whereas the nodes along both shorter boundaries were constrained to move along the y-direction. Normalized circumferential, radial and shear stresses along the hole boundary were plotted against the radial angle and found to compare well with the analytical results (Figs. 8 and 9).

4.3 Application of the Hybrid Technique to Estimate Static, and Dynamic Coefficients of Friction

This technique basically consists of applying the loading, prescribing the displacements from Moire analysis to the hole boundary and prescribing other boundary conditions as before. Thus only the plate is discretized for this analysis, without the pin, and the mesh used is shown in Fig. 10. The stresses along the boundary are obtained from the analysis and are shown in Figs. 11 and 12 plotted against the radial angle. Thus the shear stress $\tau_{r\theta}$ and the radial stress σ_{rr} show remarkable resemblence to the stresses given by Joh [2] at a load level of 1840 lbs.

In order to assess the friction coefficient values, to be used for the regular finite element analysis, $\tau_{r\theta}/\sigma_{rr}$ ratio was plotted against the radial angle for load increasing and decreasing phases and the result is given in Fig. 13. In the load increasing phase nearly all contact is associated with slip and the maximum ratio of $\tau_{r\theta}/\sigma_{rr}$ cannot exceed the dynamic friction coefficient and thus $\mu_d = 0.25$ is a rational choice. The negative ratio is maximum between 55° and 60°, where the transition from slip to stick occurs and thus $\mu_s = 0.35$ is chosen to be the static friction coefficient.

4.4 Analysis of Failure in Mechanical Joints

A composite laminate $(0°/\pm45°/90°)_s$ with laminae of the following properties has been used for these studies:

$E_1 = 19.1 \times 10^3$ ksi	$X_T = 229.4$ ksi	$T = 17.3$ ksi
$E_2 = 2.0 \times 10^3$ ksi	$Y_T = 10.1$ ksi	
$G_{12} = 0.9 \times 10^3$ ksi	$X_C = 252.1$ ksi	
$\nu_{12} = 0.3$	$Y_C = 32.0$ ksi	

It has been established that certain configurations favor certain modes of failure [18]. This fact has been used in determining the plate configurations for studying bearing failure (Mesh F, Fig. 14), shearout failure (Mesh G, Fig. 15) and tensile failure (Mesh H, Fig. 16).

The analysis has been carried out and normalized radial and circumferential strain curves have been produced for each failure mode. Failure is indicated by the increased strains given by a nonlinear model incorporating Tsai-Hill criterion as compared to a linear elastic model. Results are shown in Figure 17 for bearing failure, Fig. 18 for shearout failure and Fig. 19 for tensile failure. The Tsai-Hill criterion used in this study is,

$$\left(\frac{\sigma_1}{X}\right)^2 + \left(\frac{\sigma_2}{Y}\right)^2 + \left(\frac{\sigma_3}{Z}\right)^2 - \left(\frac{1}{X^2} + \frac{1}{Y^2} - \frac{1}{Z^2}\right)\sigma_1\sigma_2 - \left(\frac{1}{Y^2} + \frac{1}{Z^2} - \frac{1}{X^2}\right)\sigma_2\sigma_3$$
$$- \left(\frac{1}{Z^2} + \frac{1}{X^2} - \frac{1}{Y^2}\right)\sigma_1\sigma_3 + \left(\frac{\sigma_4}{R}\right)^2 + \left(\frac{\sigma_5}{S}\right)^2 + \left(\frac{\sigma_6}{T}\right)^2 \geq 1$$

where X, Y are either compressive (X_C, Y_C) or tensile (X_T, Y_T) strengths and T is the shear strength in the xy plane.

5. SUMMARY AND CONCLUSIONS

The mixed finite element model developed in [1] has been modified by incorporating a realistic interface friction conditions and a solution procedure. A dynamic as well as a static friction coefficient were used to analyze a pin-loaded plate problem for which experimental results are available. The new solution algorithm not only provides flexibility in numbering the nodes but also avoids the halt of computation due to the appearance of small terms on the leading diagonal, during the analysis. An accurate contact stress analysis is essential in some applications such as the study of failure in bolted

joints of laminated composites and some example problems have been studied in this area.

It is possible to extend the capabilities of the present model even further by adopting an Eulerian-Lagrangian formulation. This will simplify the analysis of problems, such as cracks emanating from bolted joints by several orders of magnitude.

Acknowledgements

The research reported here is supported by the Mechanics Division of the Office of Naval Research through Contract No. N00014-84-K-0552. The encouragement and support of the research by Dr. Alan Kushner is gratefully acknowledged. Thanks are also due to Mrs. Vanessa McCoy for skillful t,ping of this manuscript.

REFERENCES

1. Heyliger, P. R. and Reddy, J. N., "A Mixed Computational Algorithm for Plane Contact Problems," Computers & Structures, Vol. 26, No. 4, pp. 621-653, 1987.

2. Joh, D., "An Experimental Study of Frictional Phenomena Around the Pin Joints of Plates Using Moire Inferometry," Ph.D. Dissertation, Department of Engineering Science and Mechanics, Virginia Polytechnic Institute and State University, Blacksburg, VA, 1986.

3. Mirza, F. A., "A Solution Technique for Indefinite Systems of Mixed Finite Elements," International Journal of Numerical Methods in Engineering, Vol. 20, pp. 1555-1561, 1981.

4. Haber, R. B., "A Mixec Eulerian-Lagrangian Displacement Model for Large-Deformation Analysis in Solid Mechanics," Computer Methods in Applied Mechanics and Engineering, Vol. 43, pp. 277-292, 1984.

5. Haber, R. B. and Hariandja, B. H., "An Eulerian-Lagrangian Finite Element Approach to Large-Deformation Frictional Contact," Computers and Structures, Vol. 20, No. 1-3, pp. 193-201, 1985.

6. Koh, H. M. and Haber, R. B., "Elastodynamic Formulation of the Eulerian-Lagrangian Kinematic Description," Journal of Applied Mechanics, Vol. 53, pp. 839-845, December 1986.

7. Hyer, M. W. and Klang, E. C., "Contact Stresses in Pin-Loaded Orthotropic Plates," Report No. CCMS 84-02 and VPI-E-84-14, Virginia Polytechnic Institute and State University, Blacksburg, VA, April 1984.

8. Hyer, M. W., Klang, E. C. and Cooper, D. E., "The Effects of Pin Elasticity, Clearance and Friction on the Stresses in a Pin-Loaded Orthotropic Plate," Journal of Composite Materials, Vol. 21, pp. 190-206, March 1987.

9. Mangalgiri, P. D., "Pin-Loaded Holes in Large Orthotropic Plates," AIAA Journal, Vol. 22, pp. 1478-1484, October 1984.

10. Mangalgiri, P. D. and Dattaguru, B., "Elastic Analysis of Pin Joints in Composite Plates," Aeronautics Research and Development Board, Govt. of India, New Delhi, Rept. ARDB-STR-5014, Nov. 1980.

11. Oplinger, D. W. and Gandhi, K. R., "Analytical Studies of Structural Performance in Mechanically Fastened Composite Plates," Army Materials and Mechanics Research Center, Watertown, MA, Report M574-8, pp. 221-240, 1974.

12. Oplinger, D. W., "On the Structural Behavior of Mechanically Fastened Joints in Composites Materials," Proceedings of the Conference of Fiber Composites in Structural Design, California, pp. 575-502, 1978.

13. Lekhnitskii, S. G., Anisotropic Plates, Translated from Russian, Gordon and Breach Science Publishers, New York, 1968.

14. Mushkhelishvili, N. I., Some Basic Problems of the Mathematical Theory of Elasticity, Translated from Russian by J. R. M. Radok, Noordhoff, Groningen, Netherlands, 1963.

15. Chang, F. K., Scott, R. A. and Springer, G. S., "Strength of Mechanically Fastened Composite Joints," University of Michigan, AFWAL-TR-82-4095, July 1982.

16. Collings, T. A., "On the Bearing Strengths of CFRP Laminates," Journal of Composite Materials, Vol. 13, No. 3, pp. 241-252, 1982.

17. Garbo, S. P. and Ognowski, M., "Effect of Variances and Manufacturing Tolerances on the Design Strength and Life of Mechanically Fastened Composite Joints," McDonnell Douglas, AFFDL-TR-81-3041, St. Louis, MO, April 1981.

18. York, J. L., Wilson, D. W. and Pipes, R. B., "Analysis of the Net Tension Failure Mode in Composite Bolted Joints," Journal of Reinforced Plastics and Composites, Vol. 1, April 1982.

19. Whitney, J. M. and Nuismer, R. J., "Stress Fracture Criteria for Laminated Composites Containing Stress Concentrations," Journal of Composite Materials, Vol. 8, pp. 253-265, July 1974.

20. Wilson, D. W. and Pipes, R. B., "Analysis of the Shearout Failure Mode in Composite Bolted Joints," Proceedings of the International Conference on Composite Structures, Marshall I. H. (Ed.), Applied Science Publishers, 1981.

21. Tsiang, T. H., "Damage Development in Fiber Composites due to Bearing, Sc.D. Thesis, Department of Materials Science and Engineering, MIT,Cambridge, MA, February 1983.

22. Tsiang, T. H. and Mandell, J. F., "Bearing/Contact for Anisotropic Materials, AIAA Journal, pp. 1273-1277, August 1985.

23. Tsiang, T. H. and Mandell, J. F., "Damage Development in Bolt Bearing of Composite Laminate," AIAA Journal, pp. 1570-1577, October 1985.

24. Reddy, J. N. and Pandey, A. K., "A First-Ply Failure Analysis of Composite Laminates," Computers & Structures, Vol. 25, No. 3, pp. 371-393, 1987.

Number of nodes = 286

Number of elements = 236 (linear)

E_1 = 10,400 ksi

E_2 = 10,400 ksi

G_{12} = 3,910 ksi

ν_{12} = 0.33

Radius of the hole = 0.375 in.

Radius of the pin = 0.3745 in.

a = 1.495 in., b = 7.005 in.,

c = 1.5 in., plate thickness = 0.06 in.

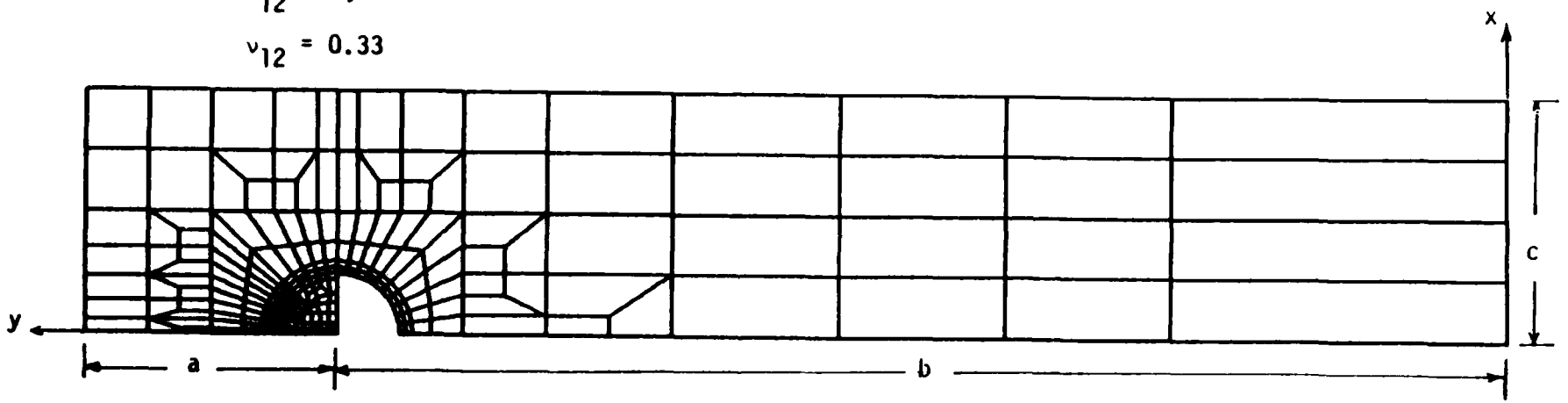

Figure 1. Mesh A for the pin-loaded aluminum plate (pin is also made of aluminum).

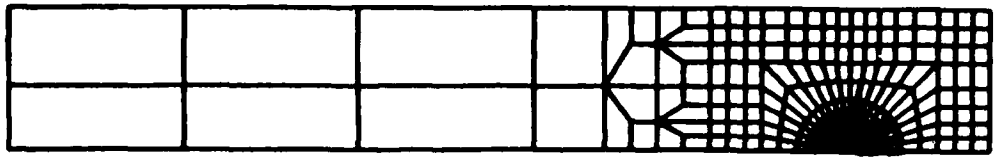

Number of nodes = 391

Number of elements = 332 (linear)

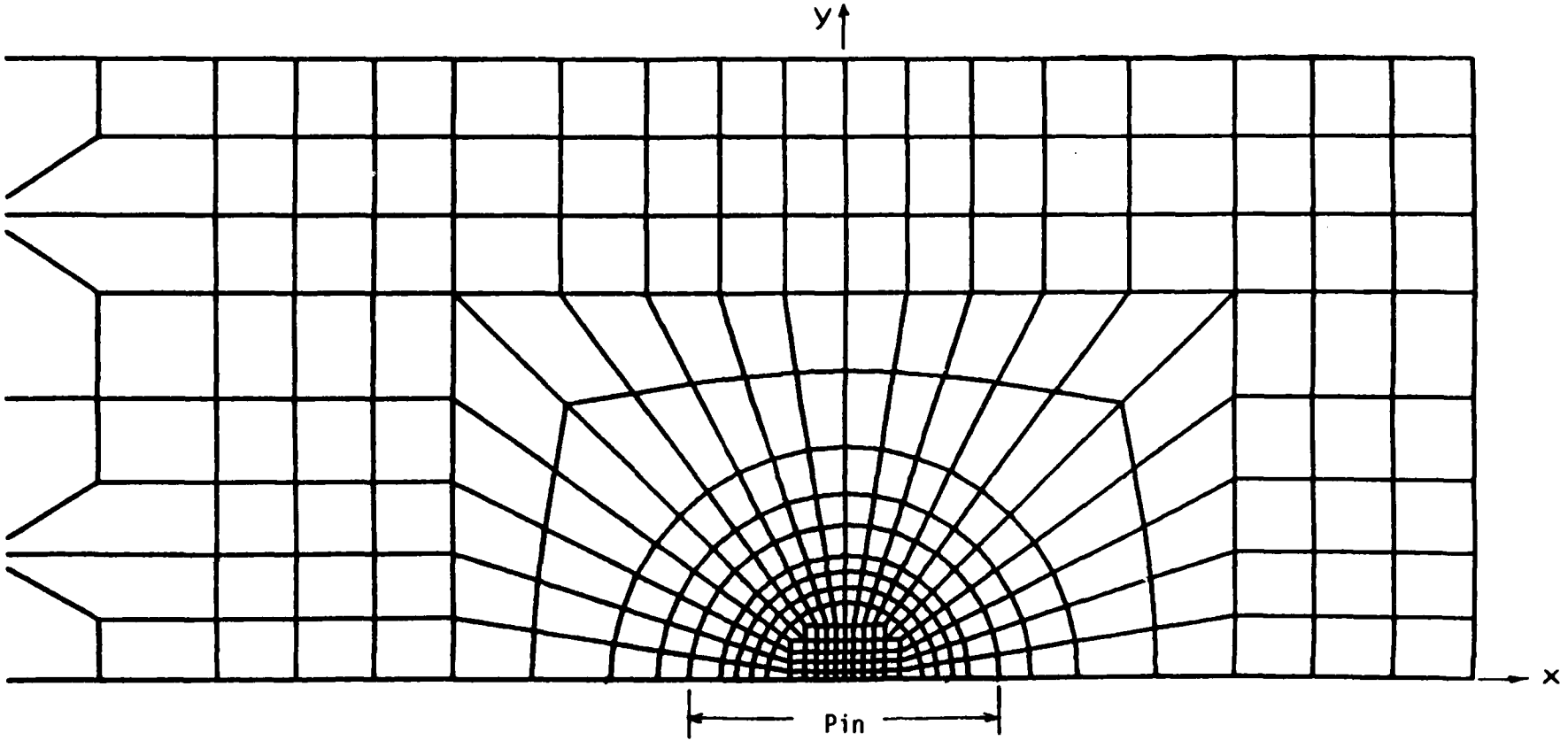

Figure 2. Mesh B for the pin-loaded aluminum plate.

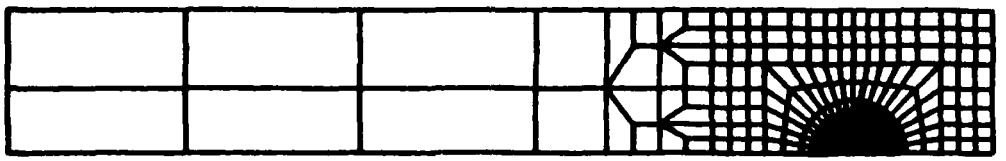

Number of elements = 540

Number of nodes = 452

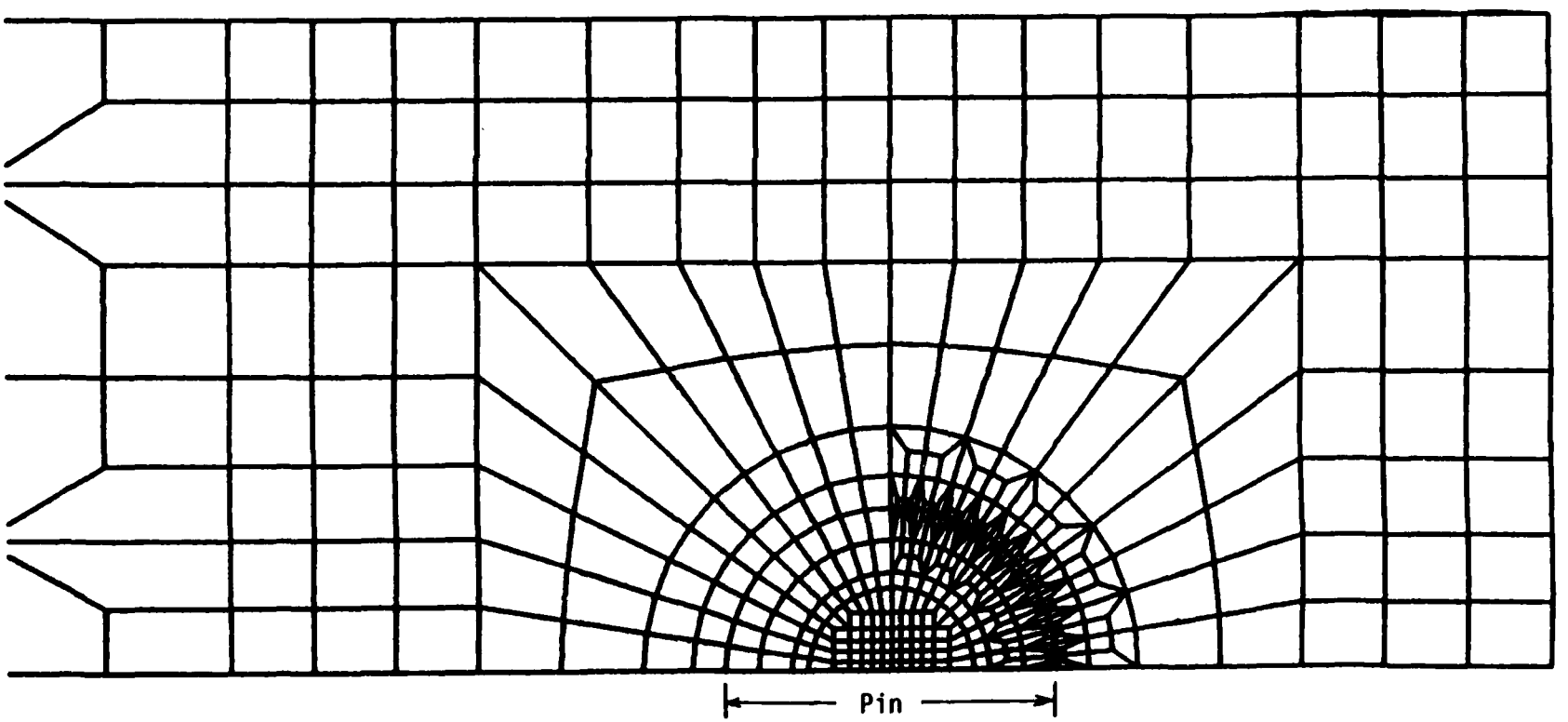

Figure 3. Mesh C for the pin-loaded aluminum plate

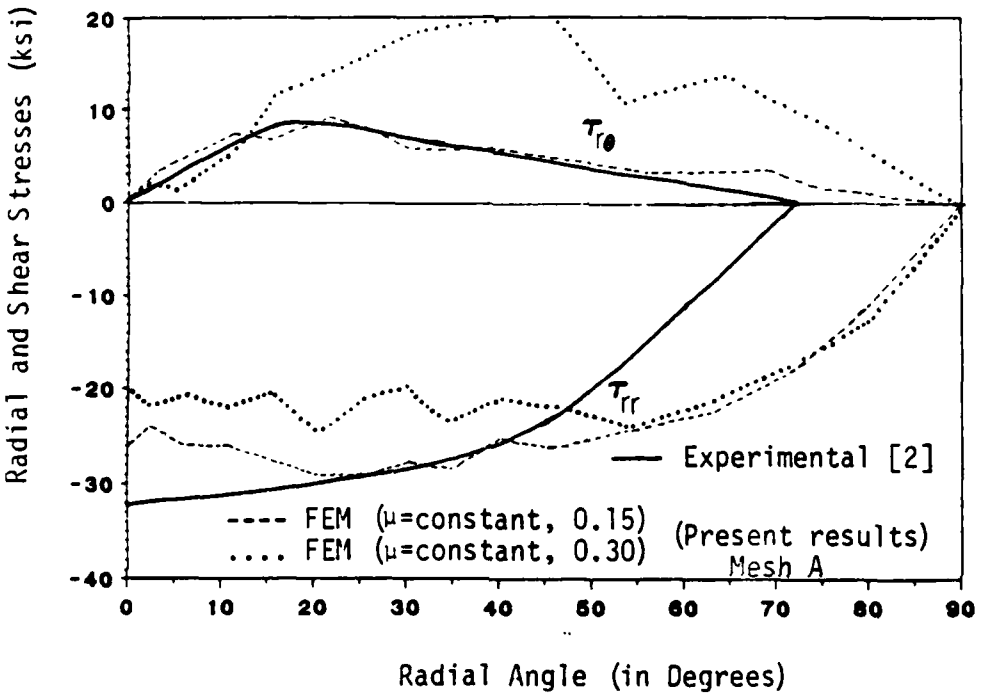

Figure 4. Comparison of the experimental and finite element results for load-increasing phase at load level 1240 lbs. (the FEM scheme used is that originally developed in [1]).

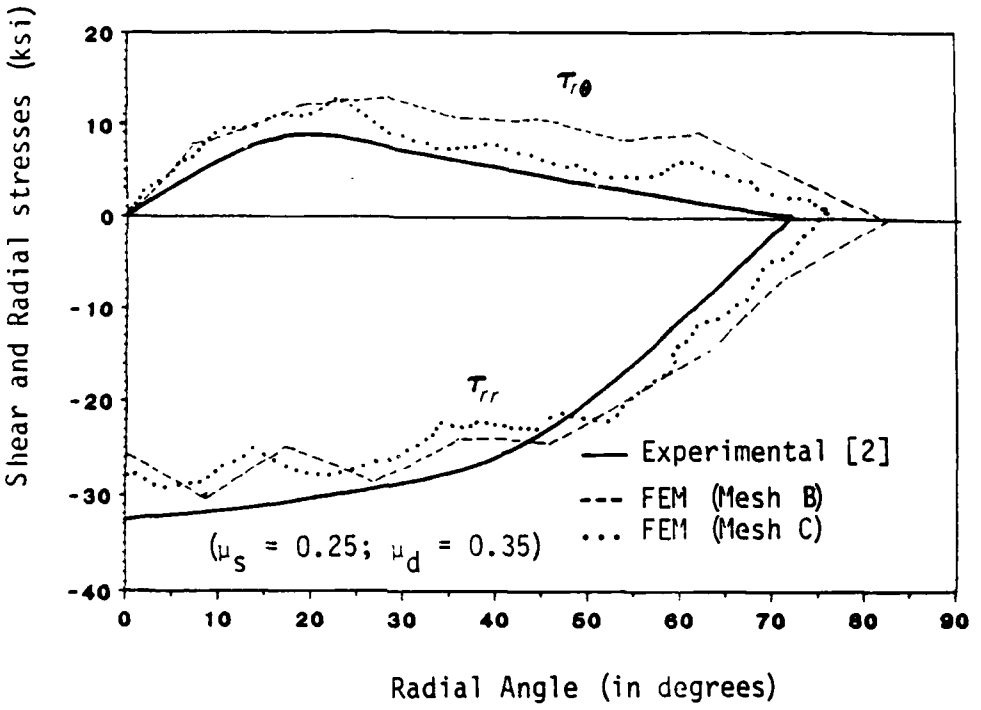

Figure 5. Comparison of the experimental and finite element results (the FEM scheme used is the modified version of the scheme developed in [1]; Load increasing phase at load level 1240 lbs.).

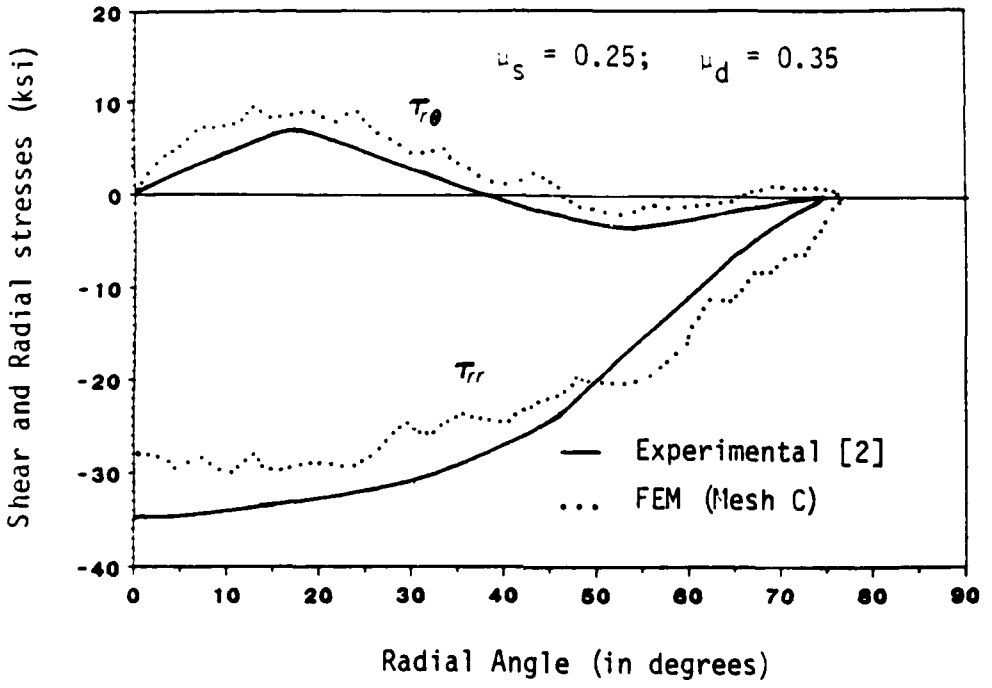

Figure 6. Comparison of the experimental and finite element results (the FEM scheme is the modified version) for the load decreasing phase at load level 1210 lbs.

Plate properties:

E_1 = 12,400 ksi

E_2 = 3,730 ksi

G_{12} = 3,210 ksi

ν_{12} = 0.66

Radius of plate hole = 1 in.
Radius of pin = 1 in.

a = 4 in., b = 2 in., thickness of plate = 1 in.

Pin is made of steel

Number of nodes = 509
Number of elements = 426

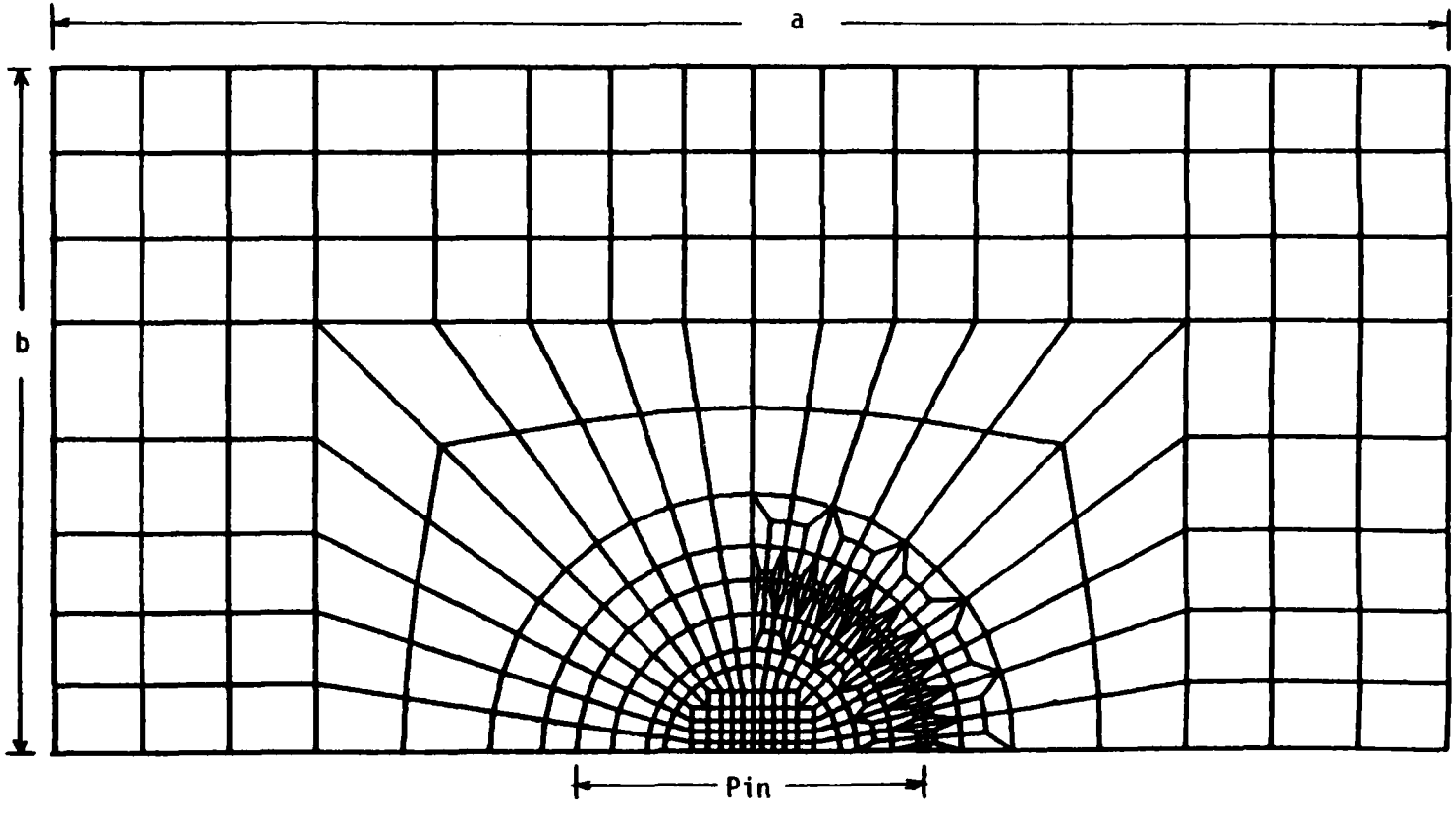

Figure 7. Mesh D for the pin-loaded orthotropic plate.

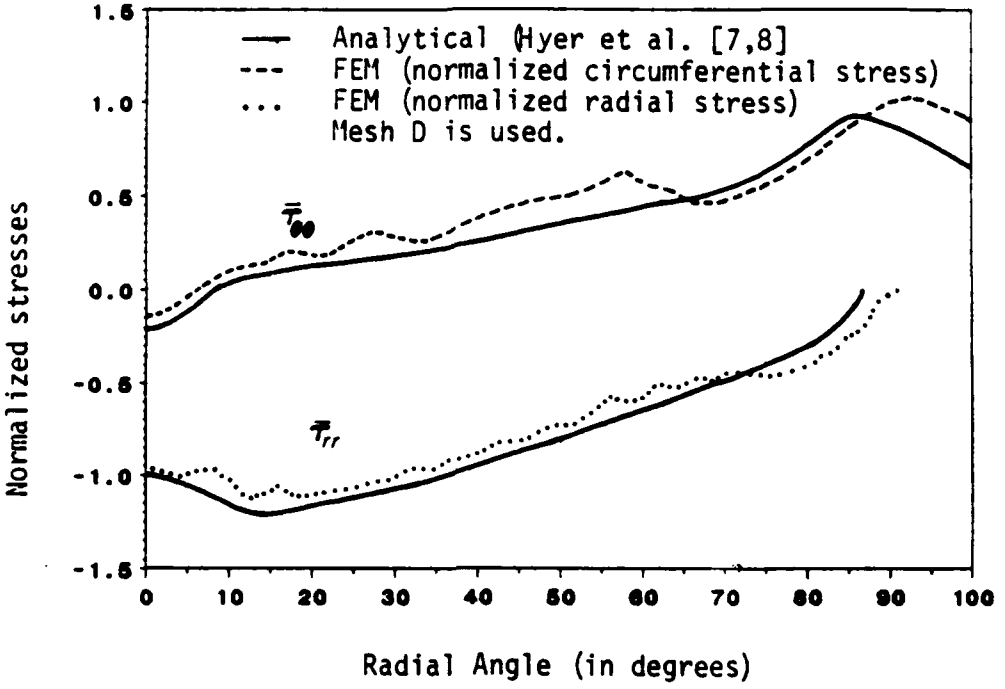

Figure 8. Comparison of the analytical and finite element results for the pin-loaded orthotropic plate. The stress is normalized with respect to the average bearing stress (81.9 ksi).

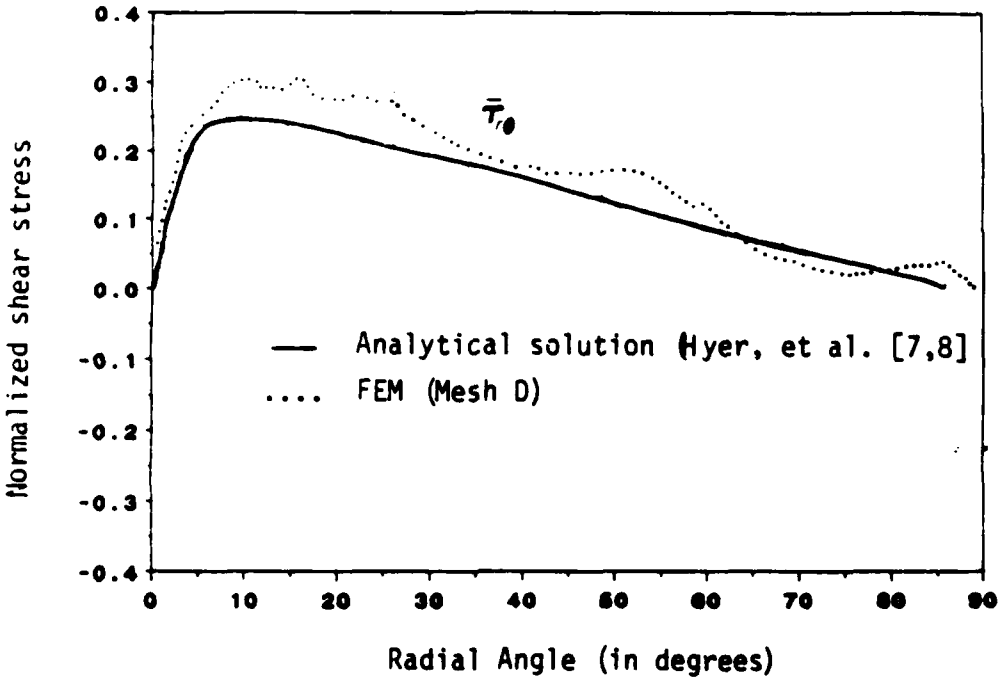

Figure 9. Comparison of the analytical and finite element solutions for the pin-loaded orthotropic plate (stress is normalized with respect to the average bearing stress, 81.9 ksi.).

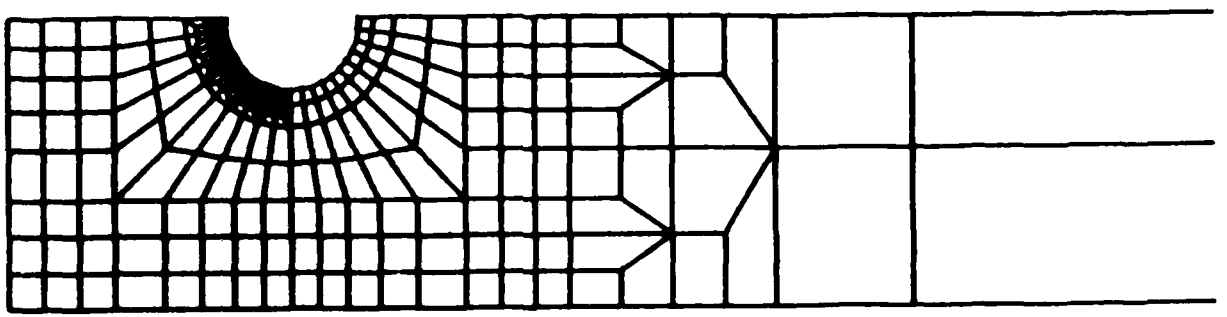

Figure 10. Mesh E used for hybrid (experimental/numerical) study of the pin-loaded plate problem.

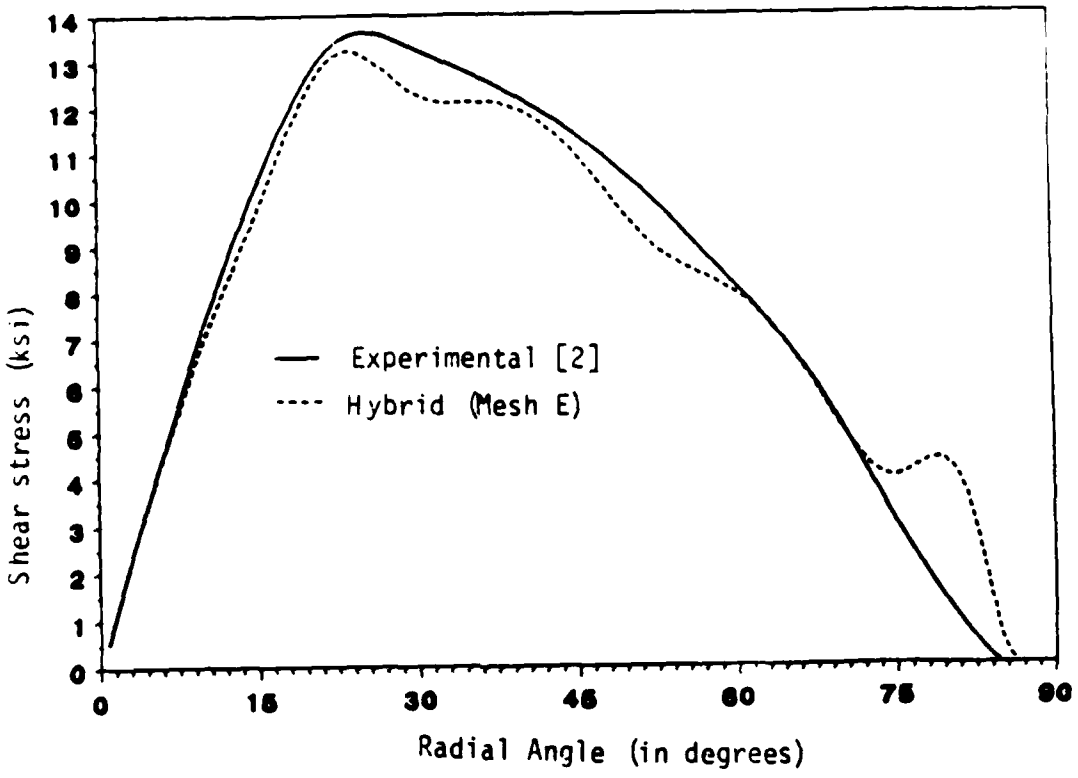

Figure 11. Comparison of the shear stress distributions obtained in the experiment and hybrid analysis of the pin-loaded aluminum plate (load increasing phase at load level 1840 lbs).

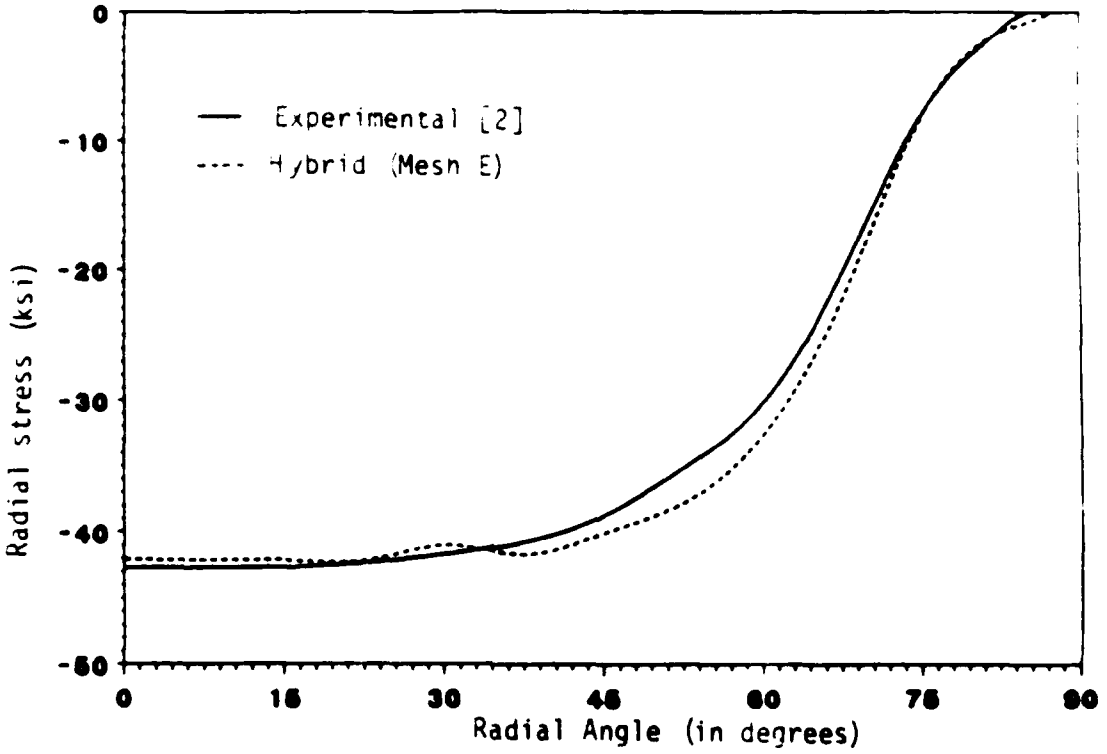

Figure 12. Comparison of the radial stress distributions obtained in the experiment and hybrid analysis of the pin-loaded aluminum plate (load=1840 lbs).

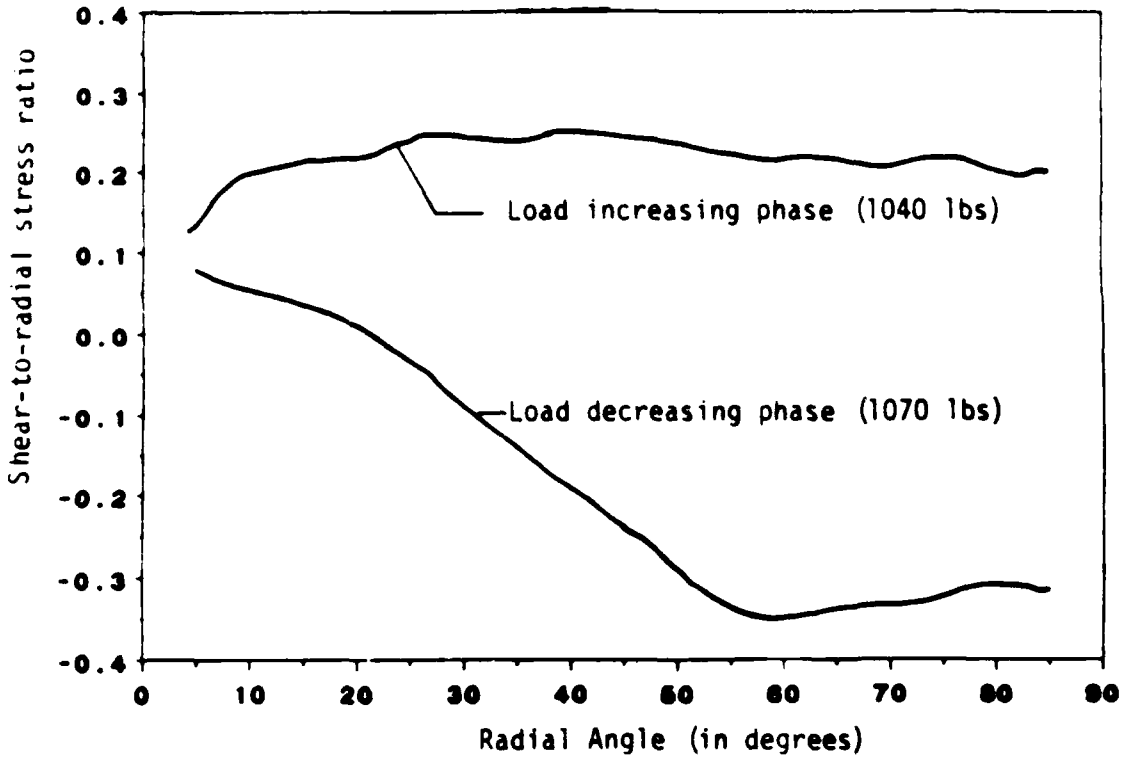

Figure 13. Variation of the ratio of shear stress-to-radial stress for load increasing and load decreasing phases of the pin-loaded aluminum plate (results obtained using the hybrid technique).

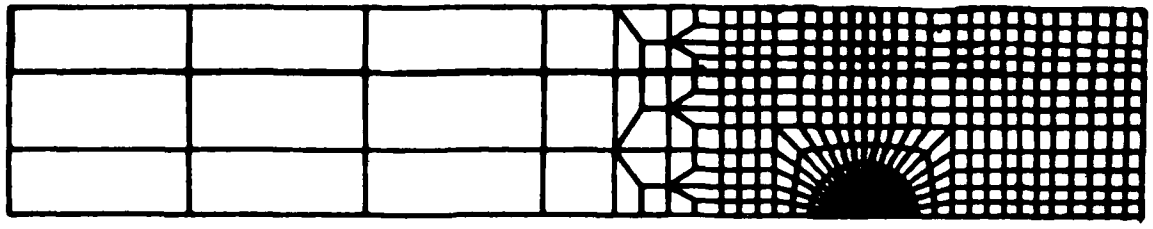

Figure 14. Mesh used for the bearing failure in a mechanical joint.

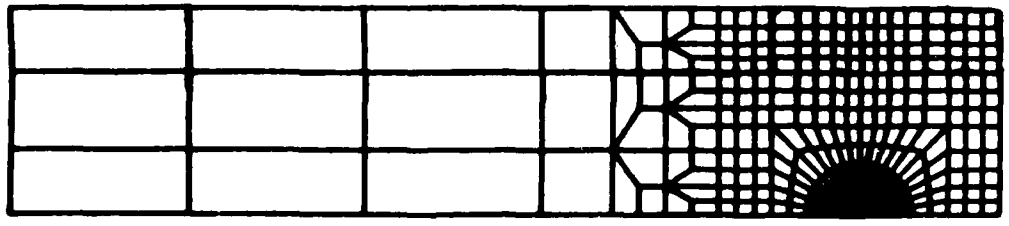

Figure 15. Finite element mesh G used for shearout and bearing failure in composite joints.

Figure 16. Finite element mesh H used in tensile failure of composite joints.

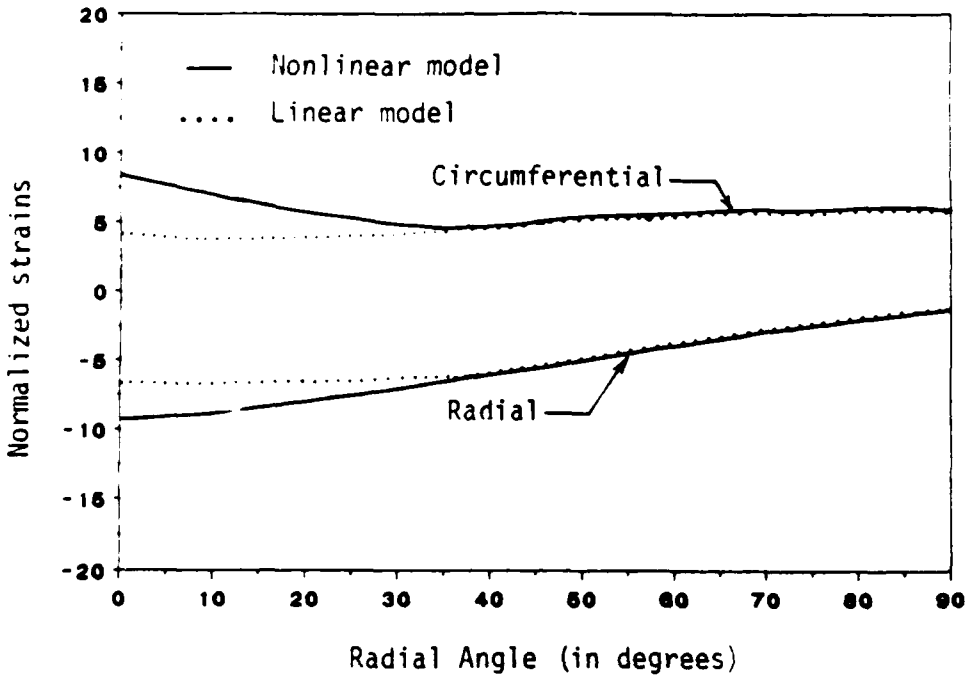

Figure 17. Radial and cicumferential strains in an orthotropic plate (the linear and nonlinear models show separation indicating bearing failure from θ=0° to θ=35°).

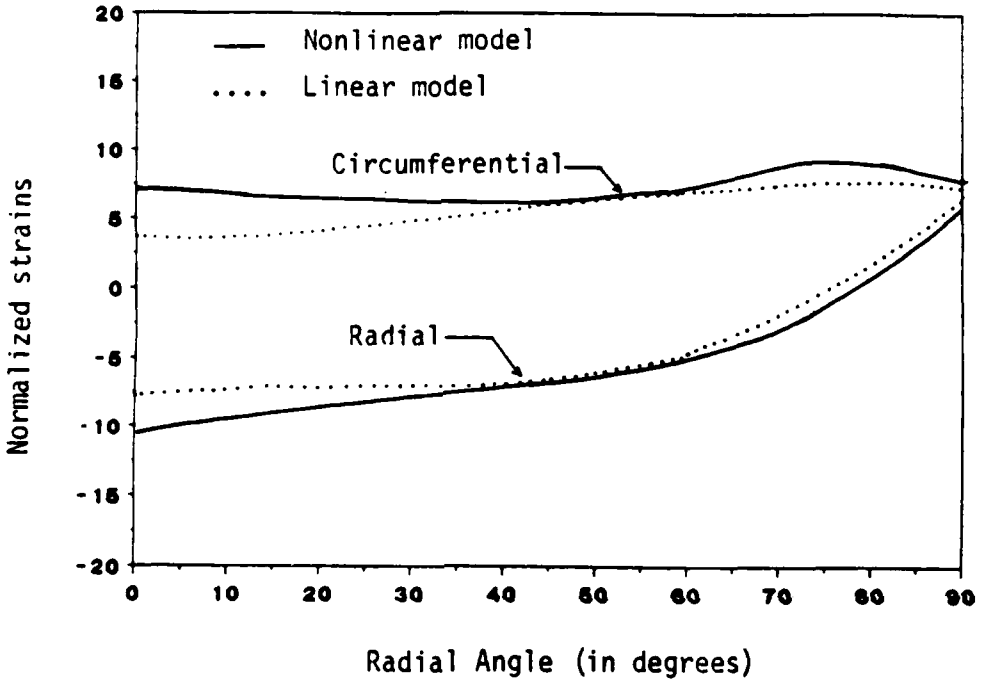

Figure 18. Radial and circumferential strains in an orthotropic plate (bearing failure: θ=0° to 35°; shearout failure: θ= 60° to 80°).

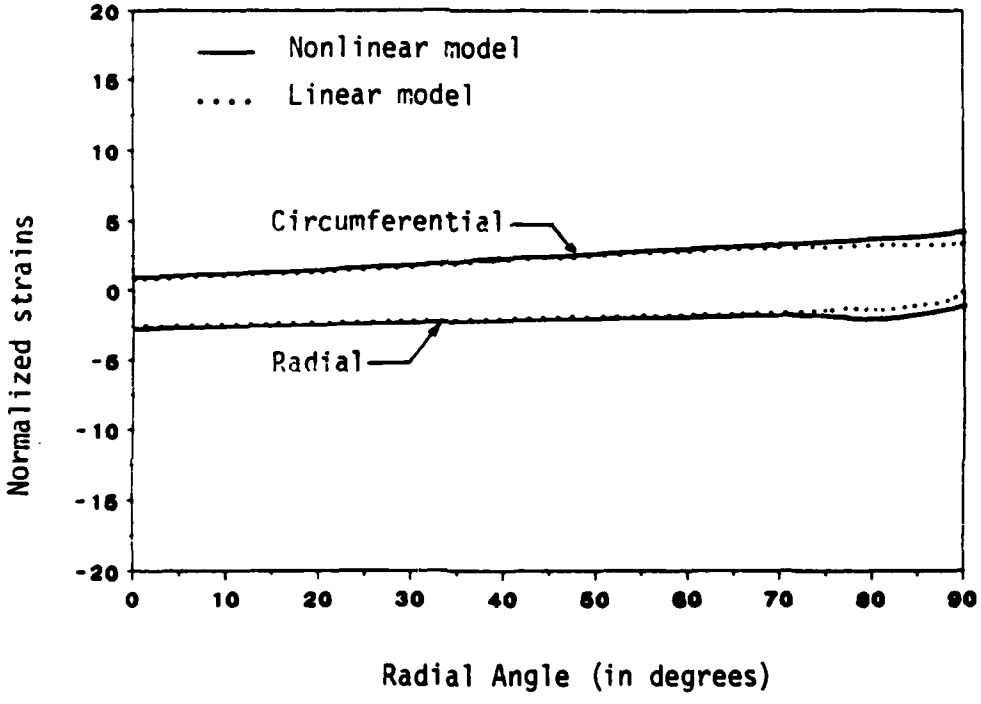

Figure 19. Radial and Circumferential strains in an orthotropic plate (tensile failure : θ = 75° to 90°).

REPORT DOCUMENTATION PAGE

READ INSTRUCTIONS BEFORE COMPLETING FORM

1. REPORT NUMBER: VPI-E-87-25	2. GOVT ACCESSION NO.
3. RECIPIENT'S CATALOG NUMBER	
4. TITLE (and Subtitle): A MIXED COMPUTATIONAL ALGORITHM BASED ON THE UPDATED LAGRANGIAN DESCRIPTION FOR PLANE ELASTIC CONTACT PROBLEMS	5. TYPE OF REPORT & PERIOD COVERED: Interim
	6. PERFORMING ORG. REPORT NUMBER: ~~ONR~~-MECH-R-4-ONR
7. AUTHOR(s): E. Yogeswaren and J. N. Reddy	8. CONTRACT OR GRANT NUMBER(s): N00014-84-K-0552
9. PERFORMING ORGANIZATION NAME AND ADDRESS: Virginia Polytechnic Institute and State University, Blacksburg, Virginia 24061	10. PROGRAM ELEMENT, PROJECT, TASK AREA & WORK UNIT NUMBERS: NR-064-727/5-4-84 (430)
11. CONTROLLING OFFICE NAME AND ADDRESS: Office of Naval Research, Mechanics Division (Code 430), 800 N. Quincy St., Arlington, VA 22217	12. REPORT DATE: October 1987
	13. NUMBER OF PAGES: 40
14. MONITORING AGENCY NAME & ADDRESS(if different from Controlling Office)	15. SECURITY CLASS. (of this report): UNCLASSIFIED
	15a. DECLASSIFICATION/DOWNGRADING SCHEDULE

16. DISTRIBUTION STATEMENT (of this Report)

This document has been approved for public release and sale; distribution unlimited.

17. DISTRIBUTION STATEMENT (of the abstract entered in Block 20, if different from Report)

18. SUPPLEMENTARY NOTES

19. KEY WORDS (Continue on reverse side if necessary and identify by block number)

contact problems, elastic-plastic analysis, Eulerian-Lagrangian formulation, finite element analysis, friction, hybrid technique, improved computational procedure, large deformations, pin-loaded plate problem, stick and slip, updated Lagrangian description.

20. ABSTRACT (Continue on reverse side if necessary and identify by block number)

The mixed finite element scheme developed earlier has been further studied in order to improve the model characteristics and operation as well as to explore further applications with regards to mechanical joints. One of the important modifications that has been implemented in the present study is the utilization of a dynamic as well as a static coefficient of friction for the evaluation of contacting surface behavior instead of a single friction coefficient as used in the previous study. This has improved the model behavior and involved a

substantial reorganization of program methodology. Other refinements include the incorporation of a modified solution technique that allows the solution of the indefinite stiffness equation system which is formed in the first iteration of the first load step, and the usage of a finer mesh. The new solution technique also avoids the halt of execution of the program whenever small elements are introduced in the leading diagonal due to contact loss.

The case of the pin-loaded aluminum plate has been studied again to obtain better correlation with experimental results; and a pin-loaded orthotropic plate behavior as predicted by an analytical solution is compared with the present model predictions. The hybrid technique has been used to estimate the static and dynamic coefficients of friction of the aluminum pin/plate system.

An elastic-plastic analysis based failure model of pin-loaded laminates is illustrated by examples which indicate when bearing, shearout and tensile failure occur in the laminate mechanical joints. Finally, some improvements that could be carried out on the present model to predict severe deformation and fracture behavior are discussed.

END
DATE
FILMD
3-88
DTIC